International Journal of Environmental Science and Technology (2022) 19:327–340
https://doi.org/10.1007/s13762-021-03173-w

ORIGINAL PAPER

Adsorption performance and Kinetics study of Pb(II) by RuO_2–ZnO nanocomposite: Construction and Recyclability

B. Mustafa[1,2] · A. Modwi[1] · M. Ismail[1] · S. Makawi[1,2] · T. Hussein[1,3] · Z. Abaker[1,4] · L. Khezami[5,6]

Received: 13 October 2020 / Revised: 26 December 2020 / Accepted: 23 January 2021 / Published online: 1 March 2021
© Islamic Azad University (IAU) 2021

Abstract

RuO_2–ZnO nanocomposite with high adsorption ability of Pb(II) was productively fabricated through mediated pectinose solution. X-ray diffraction (XRD), field emission scanning electron microscopy (FESEM), transmission electron microscopy (TEM), energy-dispersive X-ray (EDS), pore and surface area characteristics (BET), and Fourier transforms infrared (FTIR) results showed the formation of Ru-doped ZnO with new RuO_2 rutile phase. The removal kinetics process was fitted with the pseudo-second-order model. Nevertheless, the adsorption rate is possibly governed by the Pb(II) ions intra-particular diffusion. The average diameter of the nanocomposite was about 32 nm. The fabricated nanopowders have a rapid adsorption equilibrium time of 40 min and excellent competence for Pb(II) ion elimination (184.5 mg g^{-1}).

Keywords RuO_2–ZnO composite · Characterizations · Pb(ii) elimination · Recyclability

Introduction

Pb(II) ion is a substantial, mellow, elastic metal special concern because of its poisoning and its prevalent existence in the environment. Pb(II) is a famous strongly pestilent metal considered as a preference pollutant. Due to the present fast manufacturing expansion, heavy metal contamination is becoming further thought, unapproachable to the environment and community's fitness through nutrition chains (Bolan 2014). Compared to other heavy metals, Pb(II) is comprehensively and profoundly severe, spoiling the human heart, kidneys, and genital and neural systems, particularly to babies (Watt (2000)). Inorganic Pb compounds can increase in soft tissues and bones, mischievous neural framework, and give rise to serious ailment (Gloag 1981). There have previously been many ways, like adsorption, deposition, ion interchange, and reverse osmosis, which have been sophisticated to remove Pb(II) to minimize contamination (Kołodyńska 2012). Various manners have been notified in the literature to remove Pb(II) from water including sedimentation (Pan et al. 2006), percolation (Kedziorek and Bourg 2000), inverse osmosis (Bandehali 2020), ion-exchange (Cao 2019), coagulation method (Bora and Dutta 2019), and adsorption process (Ghiloufi 2019; Modwi 2017a). While some of these approaches are costly and tricky to run, the others are power-dense operations like distillation. Many investigators have been notified of traditional adsorbents' use to remove heavy minerals such as zeolites and activated carbon; however, such traditional adsorbents were notified to display little adsorption capability across heavy metal ions (Mohan 2017). Adsorption methods have several advantages, such as suppleness in process and design, and it can create treated wastes within height quality. As a result, the adsorption procedure has become one of the main techniques for eliminating heavy metals from water and wastewater. Nanomaterials that have been deliberated to remove metal ions such as ZnO, TiO_2,

Editorial responsibility: Q. Aguilar-Virgen.

✉ L. Khezami
lkhezami@gmail.com

[1] Department of Chemistry, College of Science and Arts, Qassim University, Ar Rass, Saudi Arabia

[2] Department of Chemistry, Faculty of Science and Technology, Alneelain University, Khartoum, Sudan

[3] Department of Chemistry and Biology, Faculty of Education, Al-Butana University, Khartoum, Sudan

[4] Department of Chemistry & Industrial Chemistry, College of Applied & Industrial Sciences, Bahri University, Khartoum, Sudan

[5] Department of Chemistry, College of Sciences, Imam Mohammad Ibn Saud Islamic University (IMSIU), Riyadh 11623, Saudi Arabia

[6] LaNSER, Research and Technology Centre of Energy (CRTEn), Borj Cedria Technopark, BP.95, Hammam-Lif 2050, Tunisia

(Alipour 2020; Yousefzadeh et al. 2018). The most significant inconvenience of these adsorbents comprises of its reduced adsorption effectiveness for low concentrations of heavy metals. Therefore, it is required to discover other nanocomposites with improved metal adsorption efficacy for low heavy metals in aqueous solution.

ZnO nanoparticles, fabricated by a sustainable, eco-friendly process, receive increasing attention because of their cheap cost and environmental friendliness (Zagal-Padilla and Gamboa 2018). Natural polymers, such as starch (Sagadevan 2019), pectin (Yu 2019), gelatin, or gum arabic, have been effectively used to make ZnO nanoparticles (Zak 2011; Pauzi et al. 2020). Nevertheless, there are some drawbacks to these approaches. For example, natural polysaccharides in natural polymers (such as starch, gum, and pectin) comprise metallic and nonmetallic impurities, changing the zinc's preferred properties oxide nanoparticles by polluting them with the metallic and nonmetallic elements. Hence, for the fabrication of high-quality RuO_2–ZnO nanocomposite adopting a green fabrication method, a highly uncontaminated and economical fuel is needed. In this interest, pectinose solution could be applied as a mediating material to form RuO_2–ZnO with high purity because of its low cost and facility use. Despite this, few investigations have been carried out to manufacture RuO_2–ZnO nanocomposite in the presence of a monosaccharide. Though, to the best of our information, no attempt has been dedicated to fabricated RuO_2–ZnO nanocomposite in the presence of pectinose for enhancing the adsorption performances of ZnO. Besides, the heterojunction of RuO_2–ZnO nanocomposites still needs largely studies.

Notwithstanding the obtainability of some research that was applying RuO_2–ZnO nanocomposite well-known heterojunction as an adsorbent material, only limited reports exist on the preparation of RuO_2–ZnO composite for heavy metals removal, and henceforth still additional researches have to be addressed. This limitation interested us in preparing and design; for the first time, nanomaterial comprises of RuO_2–ZnO fabricated using pectinose sugar solution, and the obtained nanomaterials were used for Pb(II) removal from queues solution. The as-synthesized RuO_2–ZnO composite showed extremely high removal competence toward Pb(II).

Materials and methods

Fabrication and characterization of RuO_2–ZnO composite

3 mmoles of Zn $(NO_3)_2{\cdot}2H_2O$ solution and 0.64 g of $RuCl_3$ were treated with 100 mL of pectinose saturation solution in a 1000-mL beaker with steady heating and stirring at 200 °C for 4 h. After that, a brown-white foam obtained was cooled at ambient temperature for 20 h. The brown-white powder was dried out and annealed 120 °C for 2 h to obtain RuO_2–ZnO nonmaterial. The phase structure was studied by XRD technique via (Bruker D8—Advance equipped) with Cu-Kα exporter (λ = 0.15418 nm). The morphology of materials prepared was evaluated through field emission scanning electron microscopy (FESEM) using JEOL, JEM-6700F. The transmission electron microscopy (TEM) using JEOL, JEM-2100 was applied to examine the structure of the RuO_2–ZnO adsorbent materials. The energy dispersive X-ray spectrometer (EDS) analysis was measured to get the nominal stoichiometry composition of the nonmaterial surfaces. The chemical bonding in the fabricated specimen before and after Pb(II) ions adsorption was recorded via FTIR analyzer, Nicolet 6700, in the interval of 4000 to 400 cm^{-1} with a resolution of 4 cm^{-1}. The Pb(II) concentration was measured by means of an ICP analyzer.

The composite zero charges points (pHPZC) determination

The RuO_2–ZnO nanomaterial zero charges point (pH_{PZC}) was assessed applying aqueous solutions of sodium chloride (0.10 mol L^{-1}) with different values of pH. The primary pH solutions were adjusted from 1 to 13 (ΔpH ~1) by means of hydrochloric acid or sodium hydroxide aqueous solutions (Damasceno et al. 2020). In typical procedure, 10 mg of RuO_2–ZnO was suspended into 10 mL of dissimilar primary pH solutions, and the mixtures were magnetically agitated (600 rpm) at ambient temperature for 1 h. Afterward, the final pH of the centrifuged liquids were determined and recorded. The primary and final pH values were measured utilizing a benchtop pH-meter. The plot of initial versus final pH values was drawn, and the pH_{pzc} value was then located.

2.3. Adsorption study

The adsorption operations were used to assess the Pb(II) adsorption parameter on the fabricated RuO_2–ZnO nanomaterials. For the contact time and kinetic study, a known volume of Pb(II) at an initial concentration of about 45 mg L^{-1} was mixed with 40 mg of the RuO_2–ZnO nanomaterials. The adsorption test was carried out in the darkness under vigorous magnetic agitation (i.e., 600 rpm). Afterward, a small volume of the mixture was extracted at incremented time intervals and then centrifuged to measure the residual metal ion amount. The amount of Pb(II) removed per gram of catalysts at any time (min) is estimated using the following expression (Modwi 2017b):

$$q_t = \frac{(C_0 - C_t)V}{w} \tag{1}$$

where q_t (in mg g^{-1}) is quantity of Pb(II) ions removed per amount of nanoparticles w (g) at any time t (min), V is the suspension volume (L), C_0 and C_t are, respectively, the concentrations Pb(II) ions, in mg L^{-1}, initially preset and at any time.

The equilibrium adsorption test was conducted in a 50-mL glass bottle, including 10 mg of nanomaterials and 25 mL of Pb(II) with concentrations 5, 15, 30, 45, 60, and 100 mg L^{-1} were added under a magnetic stirrer for 24 h. Next, in adsorption equilibrium, the suspension nanomaterials were centrifuged and filtered through a membrane filter (0.2 µ), after which the residual concentration was measured as employed in Eq. (2).

$$q_e = \frac{(C_0 - C_e)V}{w} \tag{2}$$

where q_e (mg g^{-1}) is quantity of Pb(II) ions removed by mass of nanoparticles and C_e is the concentration at equilibrium in mg L^{-1}. Langmuir and Freundlich's models are mostly adapted to set worth the reached equilibrium. These models are described in a linear and nonlinear manner to yield graphical representations of the equilibrium process.

Adsorption kinetics study

Adsorption kinetics and mechanisms study are fundamental in the uptake of heavy metals from wastewater as it supplies reliable information on the process. In such a process, experimental data are mostly represented by a pseudo-first- or pseudo-second-order kinetics model. Equation (3) represents a pseudo-first-order model of Lagergren (Lagergren 1898) with k_1 (min^{-1}) the rate constant and q_e the maximum quantity of Pb(II) adsorbed at equilibrium. The ln ($q_e - q_t$) plot against t permits the measurement of k_1 and q_e, correspondingly.

$$\ln(q_e - q_t) = \ln(q_e) - k_1 t \tag{3}$$

whereas the pseudo-second-order kinetic equation can be stated by the expression (Eq. 4), in which k_2 is the model rate constant in g mg^{-1} min^{-1} (Ho and McKay 1999,1998). Both constants q_e and k_2 can be evaluated knowing the slope and the intercept of the graph t/q_t versus t.

$$\frac{t}{q_t} = \frac{1}{k_2 \cdot q_e^2} + \frac{t}{q_e} \tag{4}$$

The initial rate of the adsorption, $h_0 = k_2 \cdot q_e^2$, can be calculated as the reciprocal value of the intercept of Eq. (4). The half time of the adsorption reaction, $t_{1/2} = 1/(k_2 \cdot q_e)$, defines the time needed for the process to uptake half amount of Pb(II) metal ion as its equilibrium state. The time is frequently hired as the removal rate quantification. Both parameters are evaluated and assembled in Table 1. The Elovich kinetic model has, as well, been successfully employed for the aqueous solution to characterize adsorption process reactions, and it is expressed as follows (Zhang and Stanforth 2005):

$$qt = \frac{1}{\beta}\ln(\alpha\beta) + \frac{1}{\beta}\ln(t) \tag{5}$$

where α and β are the Elovich model parameters, and q_t is the coverage of adsorbent surface. This model may be obtained from either the diffusion-controlled method or the reaction-controlled method. The parameter β is appropriate to the activation energies if the model is built on adsorption on the adsorbent's actively heterogeneous surface. In the case of the dispersion-controlled model, it depends on the particle and diffusion coefficient.

The metal (II) uptake can be either fitted through the mass transmission at the interface liquid–solid or via the intra-particular mass diffusion. The linearized equation of mass transfer kinetic model as proposed by Mbadcam et al. (2011) is expressed as follows:

$$\ln(C_0 - C_t) = \ln(D) + k_0 \cdot t \tag{6}$$

Table 1 Kinetics models parameters for the removal of Pb(II) by RuO_2–ZnO nanocomposite

q_e (Exp)[a] (mg g^{-1})	Pseudo-second-order				
	$t_{1/2}$ (min)	h_0 (mg g^{-1} min^{-1})	q_e(Cal)[b] (mg g^{-1})	$K_2 \times 10^4$ (g mg^{-1} min^{-1})	r^2
183.94	8.6	21.2	182.15	6.4	0.9999
Pseudo-first-order			Elovich model		
q_e(Cal)[b] (mg g^{-1})	$K_1 \times 10^3$ (min^{-1})	r^2	β	$\alpha \times 10^{-4}$	r^2
18.12	1.48	0.7916	0.052	475	0.7459

[a]Experimental data

[b]Calculated data from models

D is the mass transfer constant and k_0 (min^{-1}) the adsorption constant, Pb(II) ions may be carried from the solution bulk to the RuO_2–ZnO nanocomposites intraparticle diffusion/transport process. Sometimes, such a mechanism model is a rate-limiting stage in the sorption process. The eventuality of intraparticle diffusion is examined using the Weber and Morris diffusion model (Hameed et al. 2009; El-Sikaily 2007):

$$q_t = k_{\text{dif}} \cdot t^{1/2} + C \tag{7}$$

where C is the amplitude that provides information on the boundary layer thickness. The intraparticle diffusion constant, k_{dif} values (in mg g^{-1} $min^{1/2}$), are estimated from the slopes of the plots. The plausibility of these models is, thereafter, discussed based on the regression coefficient, r^2, values.

Equilibrium isotherms study

Adsorption isotherms can characterize the equilibrium between the adsorbed component on the adsorbent and the unadsorbed component in the solution. The widely employed isotherm equations for equilibrium data modeling are Langmuir (Langmuir 1918), Freundlich (Freundlich 1907), Temkin (Allen et al. 2004), and Dubinin–Radushkevich (D-R) (Ayawei 2015). These models are expressed as follows:

$$\frac{C_e}{q_e} = \frac{1}{q_m} C_e + \frac{1}{q_m \cdot b} \quad \text{linear form of Langmuir equation} \tag{8}$$

$$\ln q_e = \frac{1}{n} \ln C_e + \ln K \quad \text{linear form of Freundlich equation} \tag{9}$$

$$q_e = \frac{RT}{B} \ln K_T + \frac{RT}{B} \ln C_e \quad \text{linear form of Temkin equation} \tag{10}$$

$$\ln q_e = \ln q_m - \beta\varepsilon^2 \quad \text{linear form of Debinin - Radushkevich} \tag{11}$$

with $\varepsilon = RT \ln\left(1 + \frac{1}{C_e}\right)$. where q_m symbolizes the maximum quantity of the adsorbent-surface concentration equivalent to the complete monolayer coverage on the active sites (Langmuir 1918), and b represents the parameter associated to the free energy of removal. q_m and b values of can be estimated from the Langmuir model graphically, as shown in (Eq. 8), i.e., $1/q_m$ and $1/(q_m \cdot b)$ are, respectively, the intercept and the slope. The Freundlich's model constants, n and k, can be estimated from the slope and the intercept of $\ln(q_e)$ against $\ln(C_e)$ linear plot (Eq. 9). The constants K and n can be linked to the bond distribution force and the adsorptive bond, individually (Freundlich 1907). The Tempkin model infers that all the molecules heat elimination increases linearly with coverage (Allen et al. 2004). The linear shape of this isotherm can be provided through Eq. (10). B is Temkin parameter, corresponding to the sorption heat (J mol^{-1}), and K_T (L mg^{-1}) is the constant of Temkin isotherm. The constants B and K_T are specified from the slope and the intercept of q_e versus $\ln(C_e)$ graph. Dubinin–Radushkevich model is designated via Eq. (11) (Ayawei 2015), where ε is Polanyi potential, β is D-R constant, R and T are, respectively, the gas constant (8.31 J mol^{-1} k^{-1}) and absolute temperature, and $E = (2\beta)^{-0.5}$ is the mean adsorption energy.

Results and discussion

Before characterizations of the composite prepared, the suggested mechanism for the production of RuO_2–ZnO could be described as follows: Throughout boiling, the hybrid solution on the hot plate, the mixture solution of zinc nitrate, ruthenium chloride, and pectinose become concentrated on creating a uniform viscous paste. On subsequent additional warming, the zinc nitrate hexahydrates begin to break up swiftly to form up NO_2 (brownish gas), N_2, CO_2, H_2O, and extra nitrogenous gases, as illustrated beneath. In addition to the melted-viscous glue resulting in the expansion and swell to create the blackish-white color foam, while the pectinose transfers to complete carbonization via dehydration and polymerization, the reactions occur as follows:

$$\begin{aligned} 2\text{Zn}(\text{NO}_3)_{2(\text{aq})} + 2\text{RuCL}_{3(\text{aq})} + \text{C}_5\text{H}_{10}\text{O}_{5\,(\text{aq})} &\xrightarrow{200^\circ\text{C}} 5\text{C}_{\text{foam}} \\ &+ 2\text{ZnO}_{(\text{S})} + 2\text{RuO}_{2(\text{S})} + \text{N}_2 \\ &+ 2\text{NO}_{2(\text{g})} + 3\text{CL}_{2(\text{g})} + 5\text{H}_2\text{O} + \text{O}_2 \end{aligned} \tag{12}$$

$$\begin{aligned} \text{C}_{\text{foam}} + \text{ZnO}_{(\text{S})} + \text{RuO}_{2(\text{S})} + \text{O}_2 &\xrightarrow{120^\circ\text{C}} \text{CO}_2(\text{g}) \\ &+ \text{RuO}_2 - \text{ZnO nanocomposite} \end{aligned} \tag{13}$$

RuO_2–ZnO sorbent descriptions

XRD analysis

The phase structure present in the RuO_2–ZnO materials was evaluated using the XRD technique. The XRD patterns for the samples confirmed that characteristic peaks at $2\theta = 31.55°$, 34.37°, 36.17°, 47.40°, 56.53°, 62.72°, 66.30°, 68.8°, and 69.03° may be ascribed to the (100), (002), (101), (102), (110), (103), (200), (112), and (201) planes of the wurtzite hexagonal ZnO structure in agreement with the JCPDS card No. 36–1451(Elmorsi et al. 2017). Besides new peaks corresponding to $2\theta = 27.9$, 34.92, and 54.35, delineating the (110), (101), and (211) of the RuO_2 rutile phase is in agreement with (JCPDS NO 88–0322) (Zhang 2010) as displayed in (Fig. 1). These

different rutile phases of RuO_2 planes were stated by previous works (Lim 2014; Ananth et al. 2013). The mean crystallite size of nanopowders computed from the full width at half maximum (FWHM) of the diffraction peak (101) was calculated via the Scherrer equation. The values obtained of crystallite size (D) are found to be 31.87 nm.

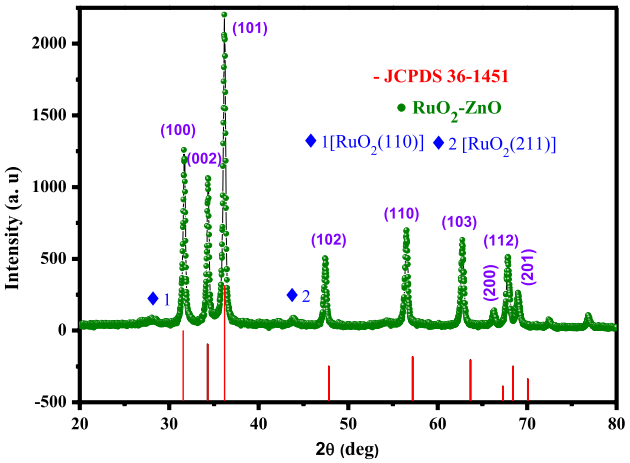

Fig. 1 XRD pattern of RuO_2–ZnO nanomaterials with JCPDS 36–1451 of ZnO

FESEM, TEM, and EDX analysis

The morphology of the RuO_2–ZnO sorbent material is demonstrated in Fig. 2a, b. FESEM with different magnifications established that RuO_2–ZnO fundamentally exists as a spherical shape of various particles size. Moreover, the TEM image's morphology of adsorbent material was also supported (Fig. 2c), which reveals oval-shaped particles with a different spherical nanoscale size. The EDX spectrum depicted weak signals at 2.5 and 0.5 keV ascribed to ruthenium (Ru) and oxygen (O). Likewise, sharp and weak peaks at 1.0 and 8.5 keV were also noticed and were due to Zn. Similar EDX results were stated for RuO_2-doped ZnO nanoparticles fabricated using wet-chemically for selective L-glutamic acid sensor (Alam et al. 2020). EDX elemental mapping analysis of Ru, Zn, and O demonstrates in Fig. 3a–c, which are displayed in distinct colors to identify their distribution within the RuO_2–ZnO nanoparticles. A brighter area in the elemental map designates a higher concentration of the conforming element. It can be observed that all elements Ru, Zn, and O are uniformly distributed over all the analyzed particles, which provides evidence for the successful synthesis of nanomaterials.

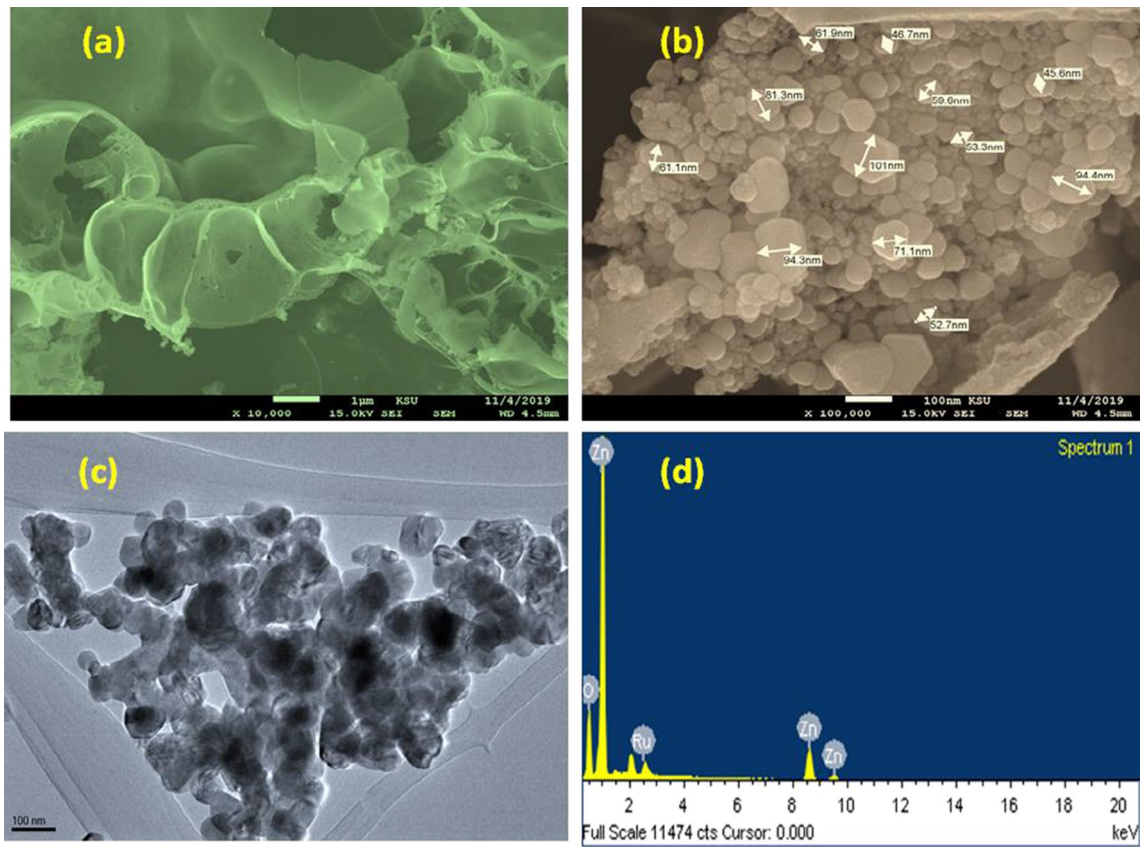

Fig. 2 The ZnO nanoparticles **a** SEM image and **b** EDX spectrum

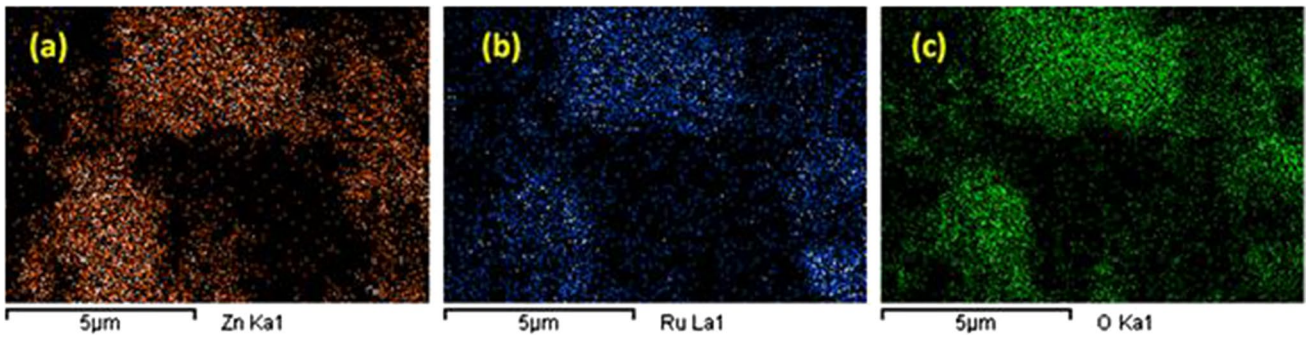

Fig. 3 The elemental mapping **a**–**c** of RuO_2–ZnO sample

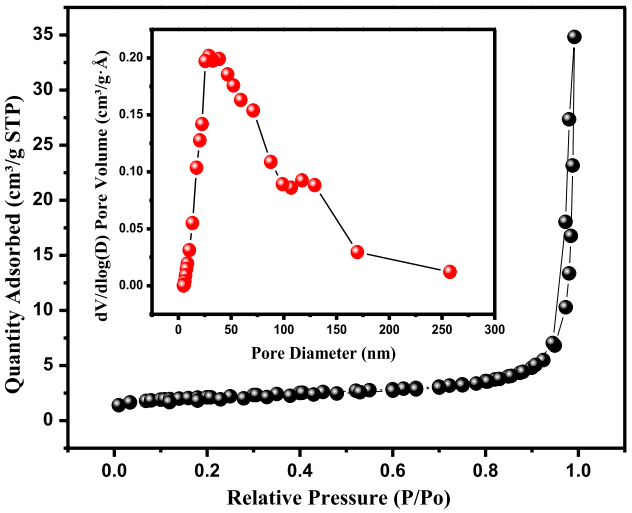

Fig. 4 N_2 sorption–desorption isotherm at − 196 °C with (inset) pore size distribution of the nanocomposite

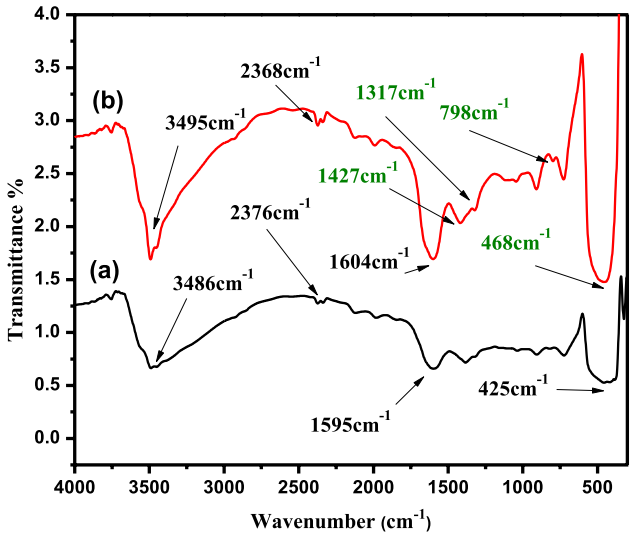

Fig. 5 FTIR spectrum of the synthesized RuO_2–ZnO nanocomposite **a** prior and **b** succeeding the removal of Pb(II) ions

Surface area analysis (BET)

The surface area pore characteristics of the as-prepared RuO_2–ZnO were determined using a Micrometrics analyzer affording BET and BJH models data. The findings gathered from the N_2 sorption isotherm verified that the isotherm is of type IV (Fig. 4). In addition, the hysteresis loop is type H3 [Fig. 4 (inset)], proving the mesoporous character of the nanomaterial including slit-shaped pores (Lippens and Boer 1965). The pore size distribution ranged from 0 to 100 nm, and the shape of the adsorption isotherm of type IV proves the mesoporous structure of the nanomaterial based on the IUPAC classification (Sotomayor et al. 2018). The BET-specific surface area of the RuO_2–ZnO composite is about 19.5 $m^2\ g^{-1}$. Besides, the pore size and volume were equal to 23.46 nm and 0.066 $cm^3\ g^{-1}$, respectively.

FTIR study

The FTIR spectra of the prepared RuO_2–ZnO nanocomposite before and after Pb(II) uptake are illustrated in Fig. 5. The stretching vibration modes of bands situated at 3410 and 1031 cm^{-1} are ascribed to the normal polymeric O–H stretching vibration of H_2O on the nanomaterials surfaces (Makeichyk 2019) due to atmospheric humidity. The sharp vibration mode at 1595 cm^{-1} owing to the H–O–H bending is assigned to a small quantity of water in the RuO_2–ZnO nanocomposite (Abdulkhair 2019). The vibration peak at 2340 cm^{-1} is accredited to the presence of CO_2 in the air (Modwi 2016). The RuO_2–ZnO bond-stretching peaks at 425 cm^{-1} designate the purity of prepared nanocomposite previously the removal process (Abdulkhair et al. 2020). The RuO_2–ZnO bond-stretching vibration modes were displaced to 468 cm^{-1} and next the removal takes place (see Fig. 5). This shift is due to the formation of new bonds of Pb–O–H

stretching vibration (Kumar et al. 2017). Similar results were stated for Pb(II) and Cd(II) adsorption onto ZnO nanoflowers (Kataria and Garg 2018). The introduction of new vibration bands at 1317 cm^{-1} belongs to Pb(II) adsorption, and the stretching vibration peak at 1427 cm^{-1} established the $Pb(OH)_2$ group on the surface of RuO_2–ZnO composite.

pH_{pzc} of ZnO nanoparticles

The zero charges point (pH_{pzc}) of nanomaterials applied in the adsorption process is an essential part that provides the pH value for which the surface charge on the composite surface will be zero. The variance within the beginning and the last hydrogen ion [H^+] or hydroxide cation [OH^-] is neutral on the surface of the adsorbent at that definite pH value (Ananth et al. 2013). Henceforth, the surface charge is further negative if $pH > pH_{pzc}$ and extra positive if $pH < pH_{pzc}$. Following, the pH of these aqueous solutions was calculated, and a plot of initial pH against ending pH was utilized to estimate the zero charges point (pH_{pzc}), as exhibited in Fig. 6. The pH at the point of neutral charges of the RuO_2–ZnO nanocomposite was found equal to 8.5.

Adsorption performance of Pb(II) ions

Effect of pH on Pb(II) adsorption

The influence of the initial pH value of the Pb(II) solution on the removal process is studied by examining seven values of pH = 2.0, 3.0. 5.0, 7.0, 9.0, 10.0, and 11.0. A 10 mg of the nanocomposite was stirred for 12 h with 25 mL as well as a 45 mg L^{-1} Pb(II) solution at room temperature. The experimental results are exemplified in Fig. 7. As shown in Fig. 7, the elimination of Pb(II) is lower at acidic pH ranging from 2 to 5; afterword, it increases to reach a maximum adsorption capacity at pH 9; subsequently, capacity drastically decreases with the increase in the pH value. The depicted high value is not only a result of adsorption but also due to the precipitation of Pb(II) at respective pH > 8 (El-Ashtoukhy et al. 2008; Faur-Brasquet 2002). The low results found at acidic pH can be ascribed to the neutralization of negative charges on the adsorbent surface, responsible for the uptake of binary positive-charged metal ions by excess hydrogen ions (El-Ashtoukhy et al. 2008). El-Ashtoukhy et al. (2008) mentioned that the maximum removal of Pb(II) ions on activated carbon was found for pH values ranging from 5.6 and 7.6.

Adsorption kinetics

Figure 8 displays the contact time effect on Pb(II) ions uptake at room temperature. The adsorption of Pb(II) metal ion on the nanocomposite was studied using stirring times in the interval of 5 to 1440 min and 45 mg L^{-1} as initial concentration. The metal ions' removal augmented proportionally with the contact time until reaching the equilibrium after 40 min. At the opening of the process, the elimination rate was very fast ($h_0 = 21.2$ mg g^{-1} min^{-1}), owing to the obtainability of active sites on the nanocomposite surface. After reaching the equilibrium plateau, the active sites concentration decline and the adsorption rate become very low. Hence, the Pb(II) adsorption remains invariable as time goes on. Accordingly, 40 min can be conceived as a convenient time to obtain equilibrium.

Alternatively, the adsorption of Pb(II) ions at the surface of nanocomposite may be governed by the intra-particular diffusion-transport process. The intra-particular model plot is displayed in Fig. 9d. From this figure, it may be visible

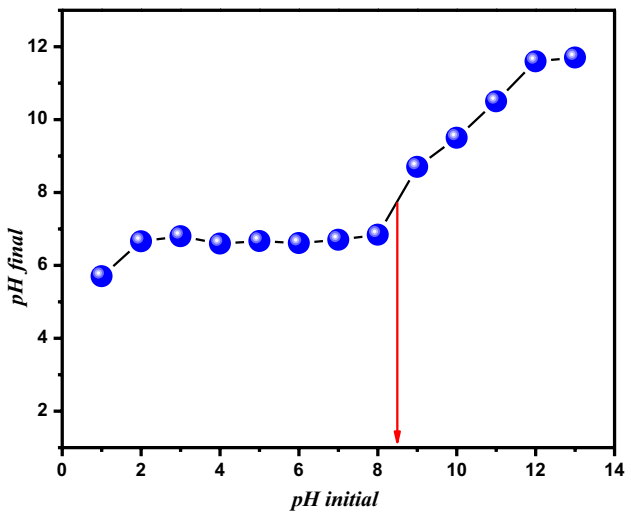

Fig. 6 pH pzc of RuO_2–ZnO nanomaterial

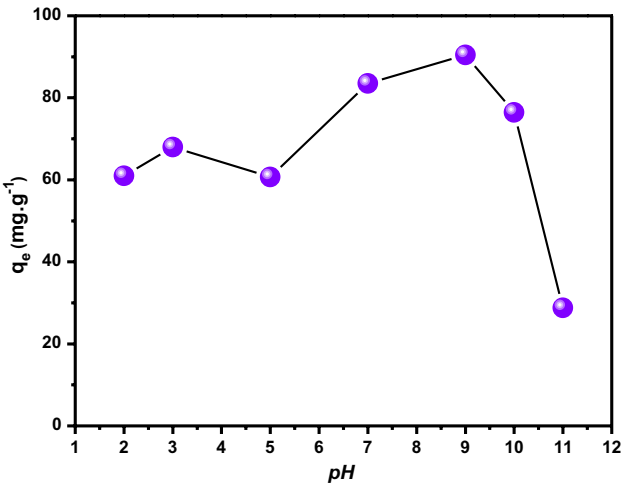

Fig. 7 Effect of pH value on the removal capacity of Pb(II) (initial concentration about 45 ppm) onto RuO_2–ZnO at room temperature

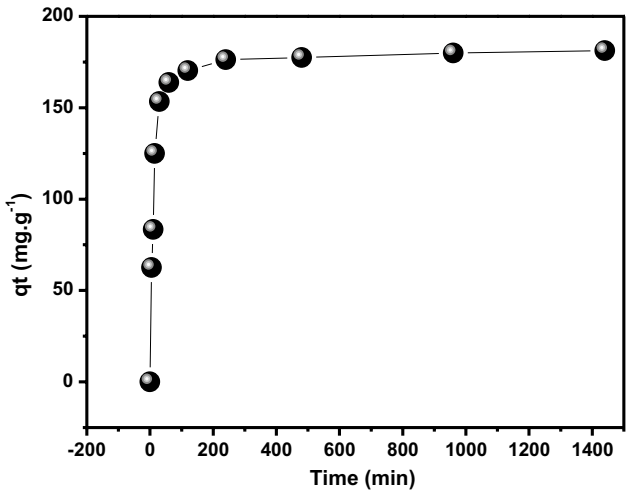

Fig. 8 Comparison of equilibrium time models for Pb(II) adsorption on RuO_2–ZnO nanocomposites, nonlinear plot

that there are two separate stage sorption, i.e., multi-linear in the case of RuO_2–ZnO (El-Sikaily 2007; Royer 2009).

The graphs in Fig. 9a of ln $(q_e - q_t)$ versus t depict linearity with correlation coefficients r^2 value less than 0.80. Besides, the calculated value of q_e is by far less than the obtained experimental values (Table 1). The Elovich model or chemisorption model also does not fit well the adsorption data performed versus time (Fig. 9c), and the found regression coefficient is about 0.75 (Table 1). However, the pseudo-second-order model diagram of t/q_t in contradiction of time (Fig. 9b) shows a better fitting for the data with a regression coefficient close to the unit ($r^2 = 0.99997$). Furthermore, *the qe* value calculated from this equation's linear plot is almost equal to that obtained from the experiments (Table 1). The pseudo-second-order model can be estimated as the best model for the kinetic profile on connecting the fitting of the applied kinetic models.

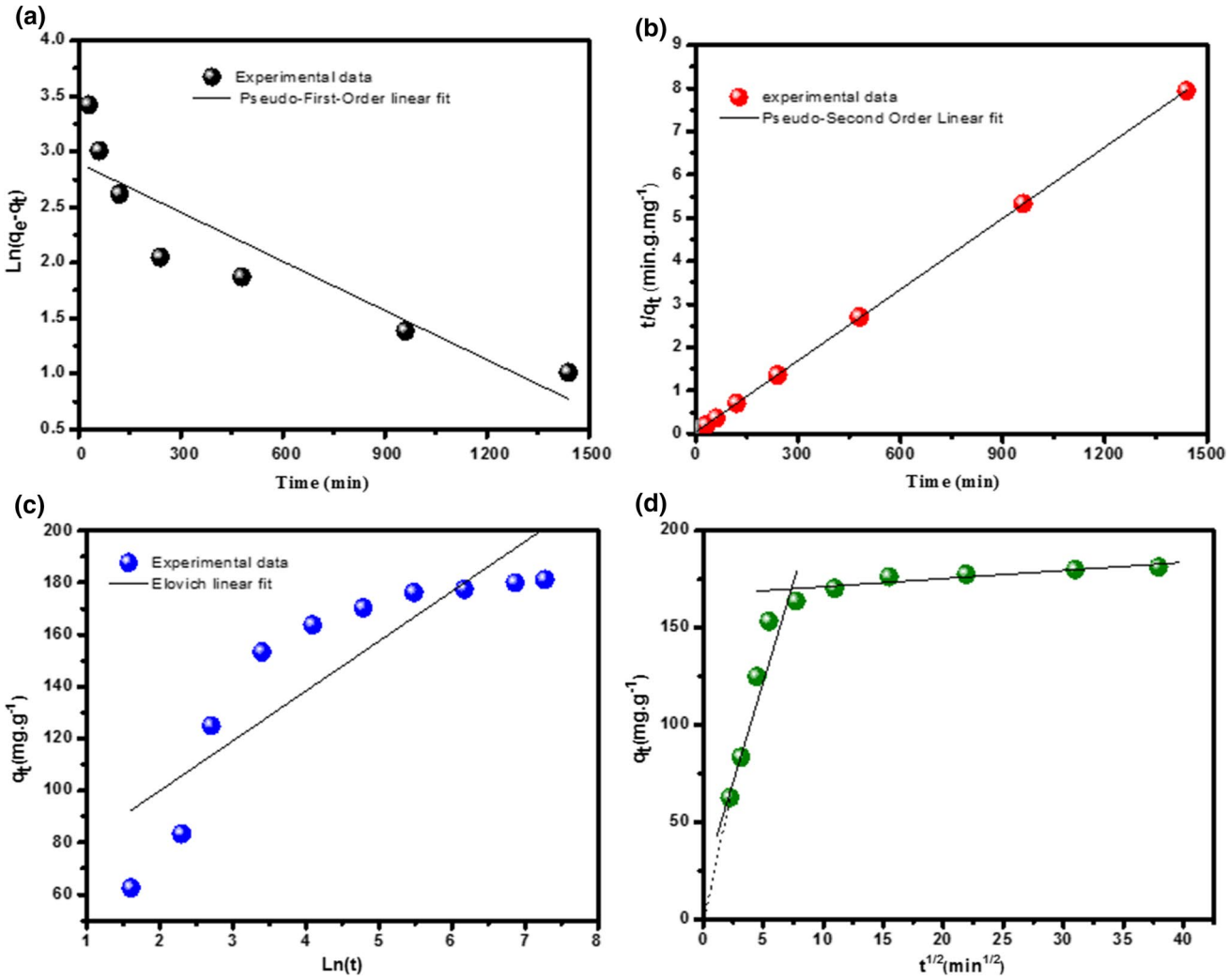

Fig. 9 **a** Pseudo-first-order **b** Pseudo-second-order, **c** Elovich kinetic models for removal **d** Intraparticle diffusion plots of Pb(II) on RuO_2–ZnO nanocomposites

The mass transfer kinetic model constants are estimated from the slope and the intercept of the straight line of $\ln(C_0 - C_t)$ against t. Though no linear relation was noticed, and the regression coefficient is mainly very low (0.44). This result designates that the sorption process rate is not controlled by mass transfer throughout the liquid film boundary.

The first straight portion, a sharp one, can be attributed to Pb(II) ions carriage across the solution bulk to the external surface of the nanocomposite through the boundary layer, macropore diffusion (Allen et al. 1989). In the meantime, the second linear portion may mention the final equilibrium where the intraparticle diffusion slowdown, owing to the low concentration of Pb(II), meso- and micropore diffusion (Allen et al. 1989). This guides to the suggestion that the adsorption can follow multiple-sorption-rates. In the same figure, the trend line is plotted and does not pass through the origin. This observation can be ascribed to some level of boundary layer monitoring. Such a phenomenon shows that intraparticle diffusion is not the only rate-governing stage, as other kinetic processes may influence the adsorption rate.

In other words, all of these operations are running simultaneously and cannot be ignored (Royer 2009). The intraparticle diffusion main parameters are evaluated and listed in Table 2. The values of intercept C, the thickness of the boundary layer, in Table 2, indicate the resistance to the external mass transfer. The constants' higher values reflect more significant effects of the solution boundary layer (Hameed et al. 2009; El-Sikaily 2007).

Adsorption equilibrium isotherms

Generally, the adsorption isotherms provide information about the uptake process of heavy metal ions at equilibrium conditions. Moreover, it manifests how metal ions are segregated between the nanocomposite surface and solution bulk at equilibrium incremented by Pb(II) ions concentration. The adsorption process is realized in batch mode through mixing10 mg of RuO_2–ZnO nanocomposite with 25 mL of a Pb(II) metal ions solution at different initial known concentrations and constant pH in a 100-mL conical flask. Numerous flasks are positioned in a multiposition agitator at 550 rpm for 12 h of interaction. 10 mL of suspension is sucked from the containers and centrifuged, then filtered employed an appropriate filter paper. The equilibrium concentration of Pb(II), Ce, in the residual filtrate is measured using an ICP. Figure 10 displays the adsorption equilibrium isotherms of Pb(II) ions eliminated by RuO_2–ZnO nanocomposite at room temperature.

Furthermore, the experimental data were fitted by the previously designated models utilizing the least-squares method. The linearized Langmuir, Freundlich, Temkin, and D-R isotherms of Pb(II) ions in solutions are drawn. As a result, the respective model constants (q_m, K_L, K_F, n, B, K_T, ε, and β) with a correlation coefficient (r^2) are calculated and gathered in Table 3.

The equilibrium parameter, R_L, is an essential characteristic attributed to the Langmuir isotherm, which is a dimensionless constant that refers to a separation factor (Zagal-Padilla and Gamboa 2018).

$$R_L = \frac{1}{1 + b \cdot C_0} \tag{14}$$

R_L value points out the adsorption nature as permanent if $R_L = 0$, linear if $R_L = 1$, unfavorable if $R_L > 1$, and favorable if $0 < R_L < 1$.

Considering the regression coefficient high values close to the unit ($r^2 = 0.9933$) as illustrated in Table 3, it can be assumed that the Langmuir model suits well the metal ions adsorption data at equilibrium (see Fig. 11a and Table 3). Based on this result, it can be said that the experimental adsorption data are adequately represented by Langmuir isotherm than that of the other models' isotherms, particularly Freundlich. Moreover, the maximum monolayer coverage capacity (q_m) estimated from the Langmuir isotherm model is about 184.5 mg g^{-1} and R_L is equal to

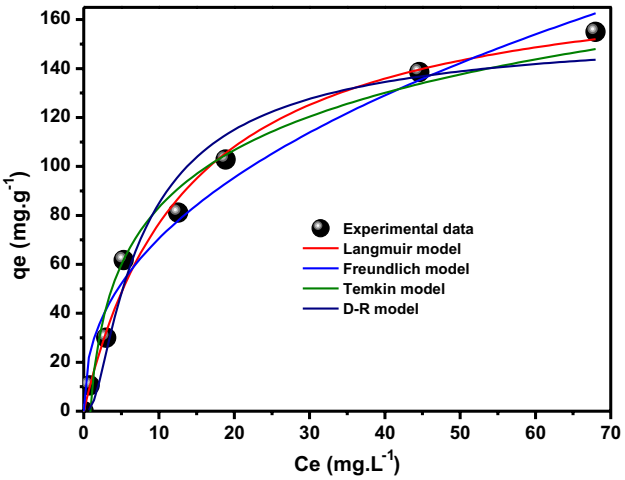

Fig. 10 Assessment of equilibrium isotherm models for Pb(II) removal on nanocomposite, nonlinear plot

Table 2 Intraparticle model parameters for the adsorption of Pb(II) by RuO_2–ZnO nanocomposite

Adsorbent	K_{1diff} (mg g^{-1} $min^{1/2}$)	C_1	r^2	K_{2diff} (mg g^{-1} $min^{1/2}$)	C_2	r^2
RuO_2–ZnO	18.65	33.66	0.9475	0.23	172.64	0.9834

Table 3 Different model isotherm constants for Pb(II) adsorption onto nanomaterial

Langmuir				Freundlich		
q_m(mg g^{-1})	B (mg g^{-1})	R_L(L mg^{-1})	r^2	n	K (L. mg^{-1})	r^2
184.5	0.072	0.074	0.9933	1.682	15.89	0.9345
Dubinin–Radushkevich				Temkin		
q_m(mg g^{-1})	$\beta \times 10^{-8}$ (mol $Kj^{-1})^2$	E (Kj/mol)	r^2	B (J mol^{-1})	K_T(L mg^{-1})	r^2
169.35	1.45	5.87	0.9869	73.5	1.225	0.9653

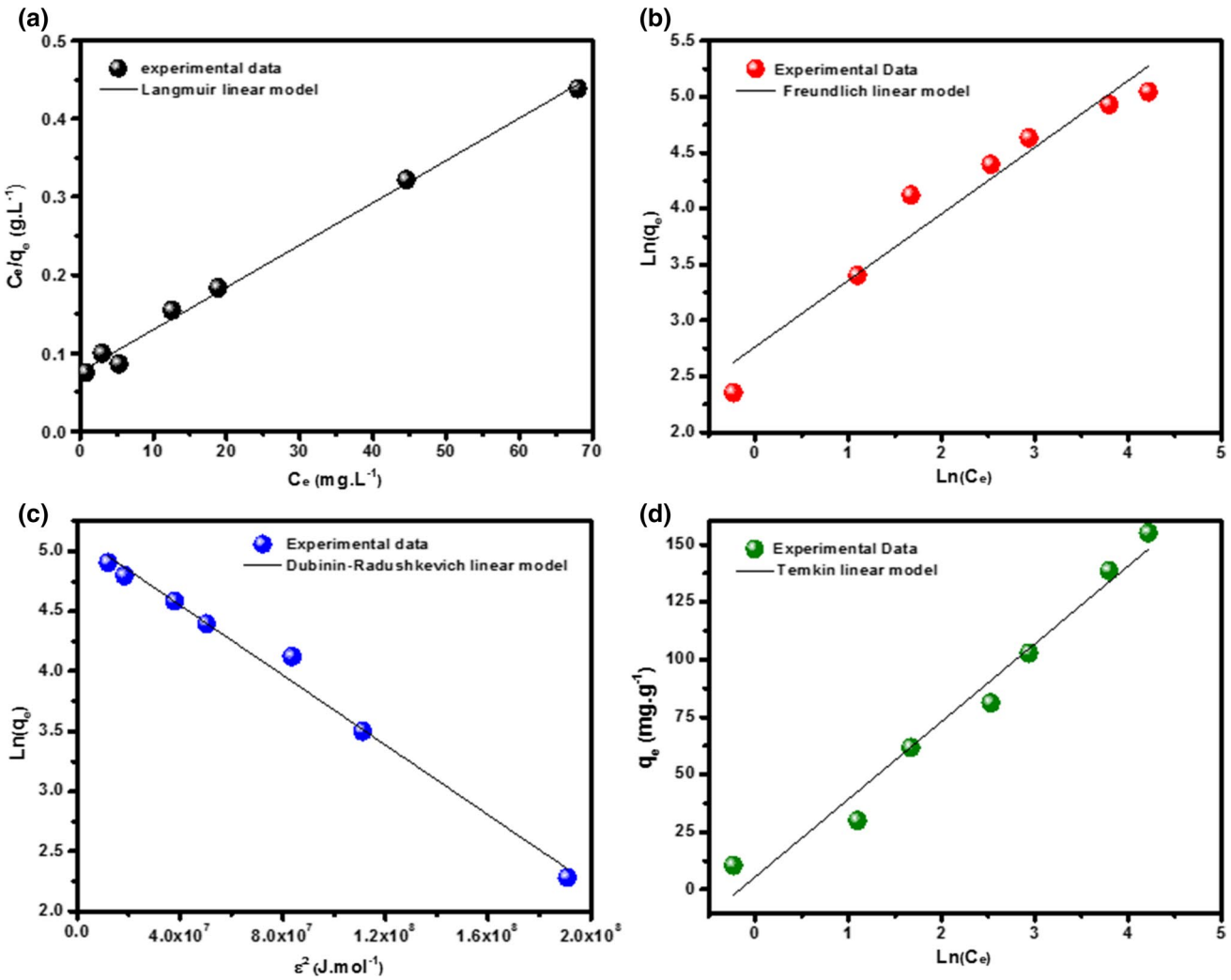

Fig. 11 Adsorption isotherm models for Pb(II) removal from aqueous solutions on RuO_2–ZnO adsorbents via batch adsorption process at 25 °C, adsorbent mass of 10 mg and using a contact time of 12 h. Comparison of isotherm models linear plot

0.074, suggesting that the adsorption process was favorable. However, based on the regression coefficient values, it should be pointed out that the D-R isotherm model described the experimental data as well (see Fig. 11c).

Recyclability and stability of the RuO_2–ZnO nanocomposite

RuO_2–ZnO nanocomposites recyclability to eliminate Pb(II) was realized for four cycles (Fig. 12). The

adsorption of Pb(II) was assessed by blending 0.1 g of RuO_2–ZnO nanocomposite with a 250 mL solution of Pb(II) (45 mg L^{-1}) for 12 h. Next, in the adsorption operation, the adsorbent was gathered utilizing a centrifuge and isolated from the suspension. The obtained material was then soaked in 50 mL of an aqueous solution of HCl, H_2SO_4, HNO_3, deionized water, CH_3COOH, C_2H_5OH, and KOH of known concentration at 25 °C at 250 rpm for 12 h in a magnetic stirrer (Rauthula and Srivastava 2011; Suresh et al. 2011). After that, the adsorbent was drained in a furnace at 105 °C for 2 h. The obtained nanomaterial was further applied for the elimination of Pb(II) ions. This process was replicated four times to estimate the reprocess competence. The removal efficacy of RuO_2–ZnO nanocomposite for Pb(II) dropped down from 92 to 61% afterward, the five cycles, as manifested in Fig. 12. Later the consequent five cycles, the subtraction settled at 61%, a sense that the RuO_2–ZnO nanocomposite fabricated employing pectinose sugar has good recyclability. The BET surface of the RuO_2–ZnO nanocomposite regenerated after the five cycles of adsorption were found to be 17.3 $m^2\ g^{-1}$, which is a negligible reduction of ≈11% compared to the surface area used in the first cycle (19.5 $m^2\ g^{-1}$).

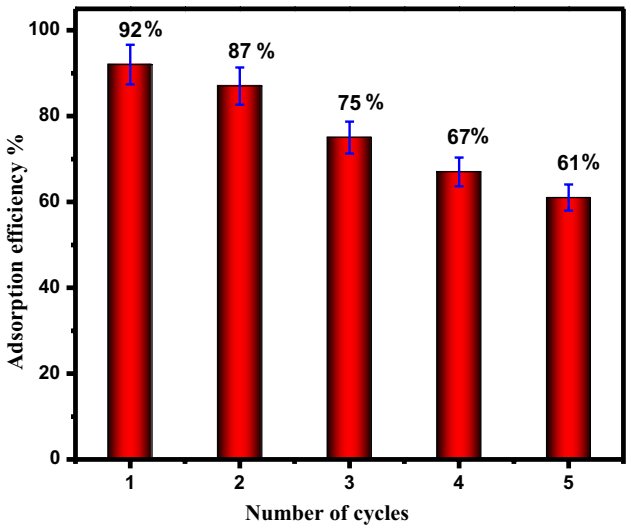

Fig. 12 The reusability of RuO_2–ZnO materials for the removal efficacy of Pb(II)

Table 4 illustrates a comparative study of the tested nanomaterial used to remove lead from aqueous solution with other investigations pointing out the maximum adsorption capacities and the time necessary to reach the adsorption equilibrium. The obtained results prove, eventually, that the studied RuO_2–ZnO nanomaterial not only has better efficiency, but the adsorption reaction equilibrium is also reached faster than the other nanocomposites in most cases.

Approximate cost analysis of prepared nanocomposite

Estimating the cost of preparing a new nanomaterial is of high importance in the practical and extensive application in wastewater treatment requirement. Substantial factors contributing to the cost are needed precursors, preparation process, washing, drying, annealing if required, washing, etc.

The price for various steps and estimating the total cost for the preparation of 1 g of RuO_2ZnO, nanocomposite has been evaluated to be ≈ $ 0.93 or SR 3.50 in Saudi Riyals (SR) (Table 5). The electricity cost per kWh is SR 0.32 for Governmental institutions in Saudi Arabia (https://www.se.com.sa/en-us/customers/Pages/TariffRates.aspx58). Based on the average concentration value of about 15.31 ppb Pb in wastewater (Kinuthia et al. 2020), 12 m^3 of the corresponding effluent could be treated using only 1 g of the prepared nanocomposite to be in concordance within world health organization (WHO) permissible limits for only 0.93$. Eventually, nanocomposite's preparation cost was reasonable, considering the high efficiency of removal and reusability study indicating that RuO_2ZnO composites could be reused up to five cycles to remove Pb in aqueous media.

Table 4 Evaluation of sorption equilibrium capacities and contact time with RuO_2–ZnO nanomaterials for Pb(II) elimination

Adsorbent	Removal capacity (mg g^{-1})	Contact time (min)	T (°C)	References
nFe@ZIF-8	175.43	60	20	Zhou (2020)
$MnFe_2O_4$	69	30	25	Ren (2012)
SiO_2/graphene	113.6	30	25	Hao (2012)
Ni-BC	142	600	25	Wang (2013)
Mg_2Al LDH	66.16	240	30	Zhao (2011)
RuO_2–ZnO	184.5	40	25	Present work
ZnO nanoflowers	115	120	–	Kataria and Garg (2018)
Chitosan/TiO_2	145.53	240	20	Tao (2009)

Table 5 Cost analysis of the prepared RuO_2–ZnO nanocomposite

Particulars	Sub-particulars	Cost of the used quantities	Cost to produce 1 g of RuO_2–ZnO	Cost to produce 1 kg of RuO_2–ZnO
Cost of precursors	3 mmol of $Zn(NO_3)_2{\cdot}2H_2O$ 0.64 g of $RuCl_3$ 100 mL of $C_5H_{10}O_5$	0.45 SR 0.38 SR 0.01 SR	1.58 SR	1580 SR
Preparation	Stirring + heating for 4 h [Power (Watt) × Time (h) × unit cost (SR/KWh)]/100 2 h	1.28 SR	1.28 SR	1.28 SR
Oven drying	[Power (Watt) × Time (h) × unit cost (SR/KWh)]/100	0.64	0.64 SR	0.64 SR
Total cost	2.76 SR ≈ 0.74 $	3.5 SR ≈ 0.93 $	1581.92 SR ≈ 422 $	

Hotplate stirrer 1000 W and the oven 1000 W

Conclusion

In this investigation, the productively, applicability, and efficiency of RuO_2–ZnO nanocomposite as a reused sorbent for removing Pb(II) ions from aqueous solutions is demonstrated. The kinetic study findings confirmed that Pb(II) ions removal was comparatively fast as its accomplished equilibrium in 40 min. Moreover, the kinetics adsorption process fitted the pseudo-second-order kinetics model well, whereas the Langmuir model has better modeled the obtained equilibrium data. The maximum removal capacity for Pb(II) onto RuO_2–ZnO was equal to 184.5 mg g^{-1} at neutral pH and room temperature. In the studied process, the intraparticle diffusion is not the only rate-governing stage, as other kinetic processes may influence the uptake of Pb(II) ions rate.

Acknowledgements The authors wish to thank all who assisted in conducting this work.

References

Abdulkhair B et al (2020) Adsorption behavior of barium ions onto ZnO surfaces: experiments associated with DFT calculations. J Mol Struct 128991

Abdulkhair BY et al (2019) Simplistic synthesis and enhanced photocatalytic performance of spherical ZnO nanoparticles prepared from arabinose solution. Zeitschrift für Naturforschung A 74(10):937–944

Alam M et al (2020) Fabrication of selective l-glutamic acid sensor in electrochemical technique from wet-chemically prepared RuO2 doped ZnO nanoparticles. Mater Chem Phys 123029

Alipour A et al (2020) Adsorptive removal of Pb(II) ions from aqueous solutions by thiourea-functionalized magnetic ZnO/nanocellulose composite: optimization by response surface methodology (RSM). Int J Biol Macromol 151:124–135

Allen S, Mckay G, Khader K (1989) Intraparticle diffusion of a basic dye during adsorption onto sphagnum peat. Environ Pollut 56(1):39–50

Allen S, Mckay G, Porter JF (2004) Adsorption isotherm models for basic dye adsorption by peat in single and binary component systems. J Colloid Interface Sci 280(2):322–333

Ananth A, Gandhi MS, Mok YS (2013) A dielectric barrier discharge (DBD) plasma reactor: an efficient tool to prepare novel RuO2 nanorods. J Phys D Appl Phys 46(15):155202

Ayawei N et al (2015) Adsorption of congo red by Ni/Al-CO3: equilibrium, thermodynamic and kinetic studies. Orient J Chem 31(3):1307–1318

Bandehali S et al (2020) Nanomaterials for the efficient abatement of wastewater contaminants by means of reverse osmosis and nanofiltration. In: Nanomaterials for the detection and removal of wastewater pollutants. Elsevier, pp 111–144

Bolan N et al (2014) Remediation of heavy metal (loid) s contaminated soils–to mobilize or to immobilize? J Hazard Mater 266:141–166

Bora AJ, Dutta RK (2019) Removal of metals (Pb, Cd, Cu, Cr, Ni, and Co) from drinking water by oxidation-coagulation-absorption at optimized pH. J Water Process Eng 31:100839

Cao Y et al (2019) Carbonization and ball milling on the enhancement of Pb(II) adsorption by wheat straw: competitive effects of ion exchange and precipitation. Bioresour Technol 273:70–76

Damasceno BS, da Silva AFV, de Araújo ACV (2020) Dye adsorption onto magnetic and superparamagnetic Fe_3O_4 nanoparticles: a detailed comparative study. J Environ Chem Eng 103994

El-Ashtoukhy E-S, Amin NK, Abdelwahab O (2008) Removal of lead (II) and copper (II) from aqueous solution using pomegranate peel as a new adsorbent. Desalination 223(1–3):162–173

Elmorsi TM, Elsayed MH, Bakr MF (2017) Enhancing the removal of methylene blue by modified ZnO nanoparticles: kinetics and equilibrium studies. Can J Chem 95(5):590–600

El-Sikaily A et al (2007) Removal of toxic chromium from wastewater using green alga Ulva lactuca and its activated carbon. J Hazard Mater 148(1–2):216–228

Faur-Brasquet C et al (2002) Modeling the adsorption of metal ions (Cu2+, Ni2+, Pb2+) onto ACCs using surface complexation models. Appl Surf Sci 196(1–4):356–365

Freundlich H (1907) Über die adsorption in lösungen. Zeitschrift für physikalische Chemie 57(1):385–470

Ghiloufi I et al (2019) Removal of lead (II) ion from aqueous solution using Ga-doped ZnO and Ca-doped ZnO nanopowder. Zeitschrift für Naturforschung A 74(7):573–580

Gloag D (1981) Sources of lead pollution. Br Med J (Clinical research ed) 282(6257):41

Hameed B, Salman J, Ahmad A (2009) Adsorption isotherm and kinetic modeling of 2, 4-D pesticide on activated carbon derived from date stones. J Hazard Mater 163(1):121–126

Hao L et al (2012) SiO2/graphene composite for highly selective adsorption of Pb(II) ion. J Colloid Interface Sci 369(1):381–387

Ho Y-S, McKay G (1998) Sorption of dye from aqueous solution by peat. Chem Eng J 70(2):115–124

Ho Y-S, McKay G (1999) Pseudo-second order model for sorption processes. Process Biochem 34(5):451–465

Kataria N, Garg V (2018) Optimization of Pb(II) and Cd(II) adsorption onto ZnO nanoflowers using central composite design: isotherms and kinetics modelling. J Mol Liq 271:228–239

Kedziorek MA, Bourg AC (2000) Solubilization of lead and cadmium during the percolation of EDTA through a soil polluted by smelting activities. J Contam Hydrol 40(4):381–392

Kinuthia GK, Ngure V, Beti D, Lugalia R, Wangila A, Kamau L (2020) Levels of heavy metals in wastewater and soil samples from open drainage channels in Nairobi, Kenya: community health implication. Sci Rep 10(8434)

Kołodyńska D et al (2012) Kinetic and adsorptive characterization of biochar in metal ions removal. Chem Eng J 197:295–305

Kumar V, Kumar S, Kumar D (2017) Synthesis and characterization of cadmium doped ZnO nanoparticles. In: Recent trends in materials and devices. Springer, pp 211–215

Lagergren S (1898) Kungliga svenska vetenskapsakademiens. Handlingar 24(4):1–39

Langmuir I (1918) The adsorption of gases on plane surfaces of glass, mica and platinum. J Am Chem Soc 40(9):1361–1403

Lim JY et al (2014) Highly stable RuO2/SnO2 nanocomposites as anode electrocatalysts in a PEM water electrolysis cell. Int J Energy Res 38(7):875–883

Lippens BC, De Boer J (1965) Studies on pore systems in catalysts: V. The t method. J Catal 4(3):319–323

Makeichyk V (2019) Quantum-chemical calculation of antioxidant properties of sulforaphane

Mbadcam JK, Anagho SG, Nsami JN (2011) Kinetic and equilibrium studies of the adsorption of lead (II) ions from aqueous solution onto two Cameroon clays: Kaolinite and smectite. J Environ Chem Ecotoxicol 3(11):290–297

Modwi A et al (2016) Effect of annealing on physicochemical and photocatalytic activity of Cu 5% loading on ZnO synthesized by sol–gel method. J Mater Sci Mater Electron 27(12):12974–12984

Modwi A et al (2017a) Fast and high efficiency adsorption of Pb(II) ions by Cu/ZnO composite. Mater Lett 195:41–44

Modwi A et al (2017b) Adsorption kinetics and photocatalytic degradation of malachite green (MG) via Cu/ZnO nanocomposites. J Environ Chem Eng 5(6):5954–5960

Mohan S et al (2017) Effective removal of lead ions using graphene oxide-MgO nanohybrid from aqueous solution: isotherm, kinetic and thermodynamic modeling of adsorption. J Environ Chem Eng 5(3):2259–2273

Pan J, Wang S, Zhang R (2006) A novel Pb(II)-imprinted IPN for selective preconcentration of lead from water and sediments. Int J Environ Anal Chem 86(11):855–865

Pauzi N et al (2020) Antibacterial and antibiofilm properties of ZnO nanoparticles synthesis using gum arabic as a potential new generation antibacterial agent. Mater Today Proc

Rauthula MS, Srivastava VC (2011) Studies on adsorption/desorption of nitrobenzene and humic acid onto/from activated carbon. Chem Eng J 168(1):35–43

Ren Y et al (2012) Adsorption of Pb(II) and Cu(II) from aqueous solution on magnetic porous ferrospinel MnFe2O4. J Colloid Interface Sci 367(1):415–421

Royer B et al (2009) Applications of Brazilian pine-fruit shell in natural and carbonized forms as adsorbents to removal of methylene blue from aqueous solutions—Kinetic and equilibrium study. J Hazard Mater 164(2–3):1213–1222

Sagadevan S et al (2019) Tailoring the structural, morphological, optical, thermal and dielectric characteristics of ZnO nanoparticles using starch as a capping agent. Results Phys 15:102543

Sotomayor FJ, Cychosz KA, Thommes M (2018) Characterization of micro/mesoporous materials by physisorption: concepts and case studies. Acc Mater Surf Res 3(2):36–37

Suresh S, Srivastava V, Mishra I (2011) Isotherm, thermodynamics, desorption, and disposal study for the adsorption of catechol and resorcinol onto granular activated carbon. J Chem Eng Data 56(4):811–818

Tao Y et al (2009) Removal of Pb(II) from aqueous solution on chitosan/TiO_2 hybrid film. J Hazard Mater 161(2–3):718–722

Wang Y et al (2013) Adsorption of Pb(II) from aqueous solution to Ni-doped bamboo charcoal. J Ind Eng Chem 19(1):353–359

Watt G et al (2000) Public health implications of new guidelines for lead in drinking water: a case study in an area with historically high water lead levels. Food Chem Toxicol 38:S73–S79

Yousefzadeh H, Salarian A, Kalal HS (2018) Study of Pb(II) adsorption from aqueous solutions by TiO2 functionalized with hydroxide ethyl aniline (PHEA/n-TiO2). J Mol Liq 263:294–302

Yu N et al (2019) New pectin-induced green fabrication of Ag@ AgCl/ZnO nanocomposites for visible-light triggered antibacterial activity. Int J Biol Macromol 141:207–217

Zagal-Padilla C, Gamboa S (2018) Optoelectronic characterization of ZnO obtained by green synthesis of Zn-salt precursor in parsley extract. J Alloy Compd 767:932–937

Zak AK et al (2011) Synthesis and characterization of ZnO nanoparticles prepared in gelatin media. Mater Lett 65(1):70–73

Zhang J, Stanforth R (2005) Slow adsorption reaction between arsenic species and goethite (α-FeOOH): diffusion or heterogeneous surface reaction control. Langmuir 21(7):2895–2901

Zhang B et al (2010) Electrochemical synthesis of catalytically active Ru/RuO2 core− shell nanoparticles without stabilizer. Chem Mater 22(13):4056–4061

Zhao D et al (2011) The adsorption of Pb(II) on Mg2Al layered double hydroxide. Chem Eng J 171(1):167–174

Zhou L et al (2020) A new nFe@ ZIF-8 for the removal of Pb(II) from wastewater by selective adsorption and reduction. J Colloid Interface Sci 565:167–176